

Acoustically Coupled Thickness-Mode AlN-on-Si Band-Pass Filters—Part II: Simulation and Analysis

Vikram A. Thakar, *Member, IEEE*, Wanling Pan, *Member, IEEE*, Farrokh Ayazi, *Senior Member, IEEE*, and Mina Rais-Zadeh, *Senior Member, IEEE*

Abstract—In this, the second of two papers, we present numerical simulations and comprehensive analysis of acoustically coupled thickness-mode AlN-on-Si filters. We simulate the scattering parameters of such acoustically coupled filters using commercially available finite element analysis software and compare the simulation results with a set of measurements. The simulations are in good agreement with the measurements, allowing the optimization of filter characteristics. We analyze the filter response under varying geometric parameters and demonstrate that variations in the top electrode geometry allow the design of low-loss filters (insertion loss <5 dB) with percentage bandwidth up to about 1% and ripple less than 1 dB.

I. INTRODUCTION

MICROMACHINED acoustic filters that are compact and support multiple frequencies and bandwidths are important to the next generation of communication systems. Bulk acoustic wave filters using electrically coupled resonators, such as ladder-type film bulk acoustic resonator (FBAR) filters, are in common use in commercial products and several techniques exist for their analysis [1]–[3]. In this paper, we make use of finite element analysis (FEA) to design and analyze acoustically coupled thickness-mode piezoelectric-on-substrate (TPoS) filters. In TPoS filters, multiple resonating elements are acoustically coupled through an elastic medium via evanescent waves [4]–[6]. Unlike FBAR filters, in which the passband is defined using electric coupling elements, the passband of TPoS filters depends on the dispersive propagation properties of Lamb modes and is much more challenging to accurately predict. Prior work on acoustically coupled filters has shown that the acoustic coupling between the resonators can be tuned by changing the interdigitated top electrode geometry [7]–[10]. Careful optimization of the number of interdigitated fingers, electrode width, and

pitch is necessary to obtain good passband characteristics with low insertion loss, thereby justifying a detailed analysis of filter geometry using numerical simulation tools.

In Part I of this paper [6], we presented an interdigitated thickness-mode AlN-on-Si TPoS filter at 2.877 GHz with an insertion loss of 2.4 dB and a 3-dB bandwidth of 12 MHz. In this part, we focus on the analysis of this filter and simulate its frequency response using Comsol Multiphysics FEA software (Comsol Inc., Burlington, MA). We further consider variations of design parameters, such as top electrode layout and thickness, to provide a comprehensive analysis of their effect on the filter performance, namely insertion loss and bandwidth. Finally, by taking advantage of the simulation platform, we present some filter design and optimization guidelines, which will alleviate the need for expensive and time-consuming fabrication trials.

II. FINITE ELEMENT MODELING

Fig. 1 shows a scanning electron microscopy (SEM) top view of a fabricated AlN-on-Si filter, as presented in Part I. The cross section and top views of the TPoS filter configuration are schematically shown in Fig. 2. In this configuration, a piezoelectric layer acts as the transduction layer and the overall stack thickness and material properties define the thickness-mode resonance frequency. The operating principle of these filters is discussed in detail in Part I.

The device shown in Fig. 1 was simulated with Comsol using the model presented in Fig. 2(a) and is analyzed using the piezoelectric application mode of the MEMS structural mechanics module. In this module, a multiphysics analysis is performed to solve the coupled wave equation which is obtained by considering the piezoelectric constitutive relations. A harmonic voltage $V_{in}(\omega)$ is applied to the input port while the output port is grounded as a necessary condition for the computation of the admittance parameters. To account for the energy radiating into the substrate, a perfectly matched layer (PML) boundary is implemented at the device edges [11]. As a rule of thumb, at least 10 mesh elements per unit wavelength are included for all simulations. From finite element simulations, we obtain the nodal current, which is integrated over the output electrodes to give the total displacement current. This displacement current is converted into the admittance

Manuscript received February 9, 2012; accepted June 27, 2012. This work was partially supported by the University of Michigan, the National Science Foundation (award number 1055308), and the Defense Advanced Research Projects Agency (DARPA) Analog Spectral Processors (ASP) program.

V. A. Thakar and M. Rais-Zadeh are with the Department of Electrical Engineering and Computer Science, University of Michigan, Ann Arbor, MI (e-mail: thakar@umich.edu).

W. Pan was with the Georgia Institute of Technology, Atlanta, GA. He is now with Integrated Device Technology Inc., San Jose, CA.

F. Ayazi is with the School of Electrical and Computer Engineering, Georgia Institute of Technology, Atlanta, GA.

DOI <http://dx.doi.org/10.1109/TUFFC.2012.2452>

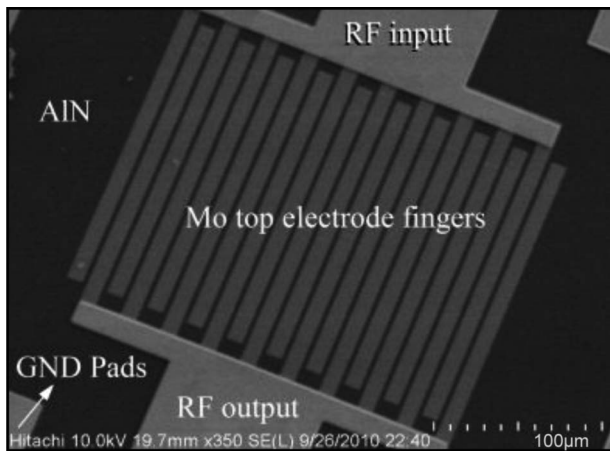


Fig. 1. A scanning electron micrograph of an acoustically coupled thickness-mode piezoelectric-on-substrate (TPoS) filter discussed in detail in Part I.

parameters, which are finally converted to S-parameters (using 50Ω termination impedance) for direct comparison with the measured filter response [12]. Because a linear and passive device is simulated, $S_{21} = S_{12}$. We also take $S_{11} = S_{22}$ because the device is symmetric. To facilitate iterative simulations and eliminate user-induced variations, the Comsol–Matlab (The MathWorks Inc., Natick, MA) interface is utilized. This setup is denoted the simulation platform or model throughout this manuscript.

A typical acoustically coupled filter as presented in this work has a minimum of 6 independent geometric design variables. These are the thickness of AlN and Si layers, thickness of the electrode layers, electrode width, number of electrode fingers, and electrode spacing. Varying the materials and material properties will add more variables, making the analysis significantly more complicated. In this work, we focus on the geometric variables—in par-

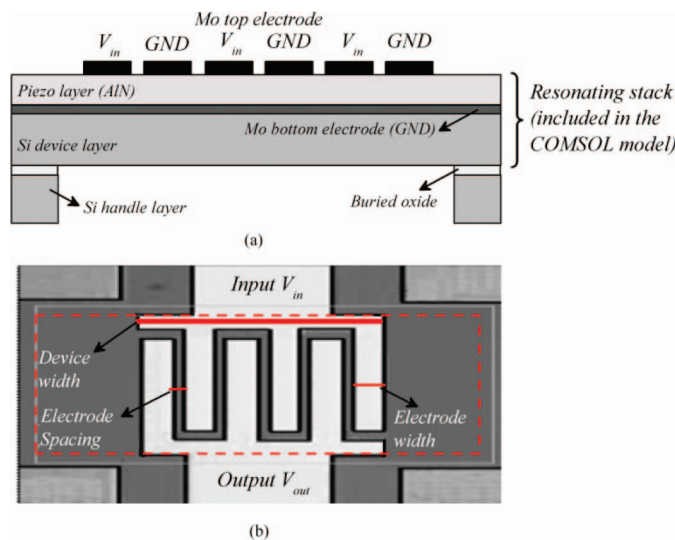


Fig. 2. (a) A cross-section schematic view of a thickness-mode piezoelectric-on-substrate (TPoS) filter showing the electrical boundary conditions used in 2-D simulations and (b) a top view showing the electrode geometric variables (only the boxed area is modeled).

ticular, on the top electrode layout. Because there is no property variation in the third dimension, i.e., the dispersion curves along this direction remain unchanged, a 2-D analysis using plain strain approximation is undertaken for reduced simulation time.

The simulated results of the thickness-mode TPoS filter shown in Fig. 1 are presented in this section as a case study. The target stack dimensions for this filter are: Mo (100 nm)/AlN (1 μm)/Mo (100 nm)/Si (5 μm). The top electrode geometry consists of 20 interdigitated fingers, each 10 μm wide with a spacing of 5 μm (pitch of 15 μm). However, the actual dimensions of the fabricated filter deviate from the target design values. In particular, film thicknesses are critical and the silicon device layer of the SOI wafer used in this work has a thickness tolerance of $\pm 0.5 \mu\text{m}$. Fig. 3 shows a cross-sectional SEM view of the wafer stack at a location near the measured filter, revealing the actual thicknesses of the AlN and Si layers. The measured film thicknesses for AlN and Si are used for the purpose of fitting the simulation results to the measured response. Initial simulations are performed, taking the generally accepted published material properties for Mo, AlN, and Si [13]. As will be seen later, the piezoelectric properties of reactively sputtered AlN deviate from the bulk values and must be accounted for in simulations. The actual properties of sputtered AlN are extracted from the fitted simulation response and are used throughout the paper to analyze the characteristics of the TPoS filters.

The simulated and measured filter responses around the fourth-order thickness mode are plotted in Fig. 4. The two simulated curves in Fig. 4 represent the results obtained using nominal design parameters and the fitted parameters. The fabricated filter response shows a slightly different center frequency and roll-off as compared with the simulated response using nominal design parameters. In addition, the measured bandwidth is narrower than the simulated one using the target design parameters. This can be attributed to variations in the geometric parameters and material properties in the fabricated device as

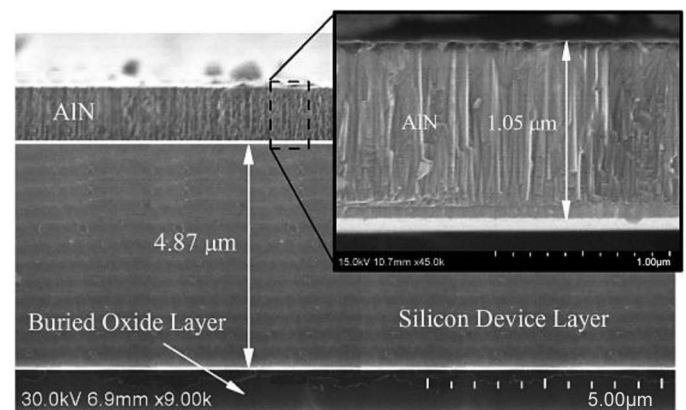


Fig. 3. A cross-sectional scanning electron micrograph of the stack. The measured film thicknesses are used in the fitted simulation. Note that the buried oxide layer is removed in the filter area. Inset shows a close-up view of the AlN film.

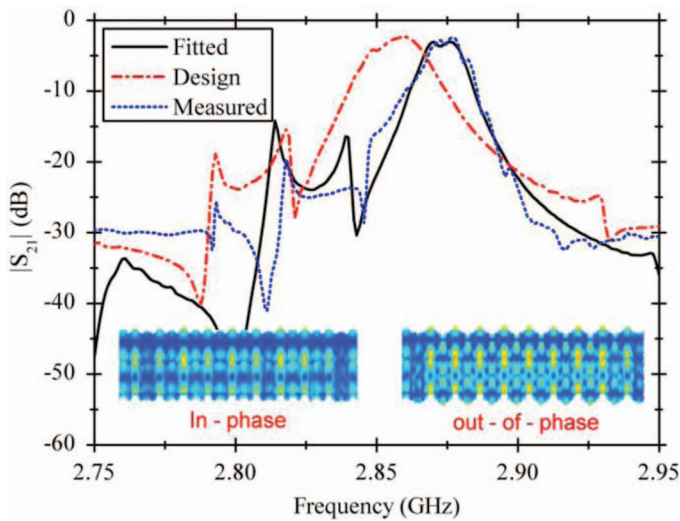


Fig. 4. Frequency response near the fourth-order thickness mode of the filter shown in Fig. 1. The design curve shows the simulation result considering the nominal design values and material properties. The fitted response involves variation of geometric parameters and the piezoelectric stress constant, e_{33} . Insets show harmonic response at in-phase and out-of-phase frequencies.

compared with target design values. With the geometric variations accounted for (through accurate SEM measurements), the difference between fitted and measured response can be attributed to variations in material properties only. Fig. 5 shows the measured and simulated (fitted) phase of S_{21} for the filter shown in Fig. 1.

In TPoS filters, the frequency separation between the in-phase and out-of-phase modes primarily determines the bandwidth, which can be tailored to a large extent by changing the layout of the top interdigitated electrodes [14]. The piezoelectric stress constant, e_{33} , through the

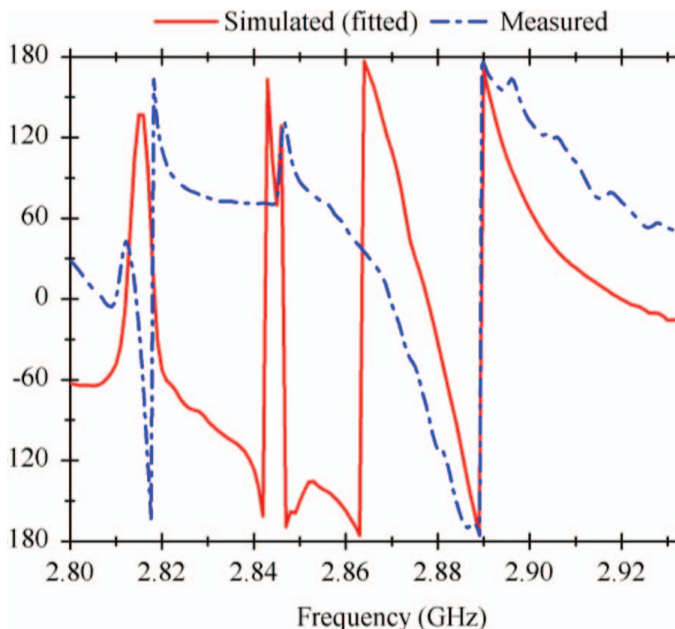


Fig. 5. The measured and simulated (fitted) phase of the filter shown in Fig. 1.

electromechanical coupling coefficient (k^2), determines the amount of energy converted from the electrical to the mechanical domain in each of the two electroded regions vibrating in thickness-extensional mode, and hence larger e_{33} values would make it possible for more charge to be collected at the output electrode with the same electric input signal. Depending on the sputtering conditions and seed material used, a wide range of e_{33} values have been measured for reactively-sputtered AlN [15], [16]. For example, e_{33} for AlN sputtered on Pt was extracted as ~ 1.43 C/m² in [15], i.e., 94% of the bulk value (1.55 C/m²). In addition, the exact orientation of the c-axis with respect to the wafer surface is not known. One can account for a non-vertical c-axis orientation by reducing the effective e_{33} value. To show the effect of e_{33} on the filter response, a set of simulations were performed by varying the AlN piezoelectric coefficient. Fig. 6 shows the response when the piezoelectric stress coefficient, e_{33} , is reduced from 1.55 C/m² to 0.8 C/m². The bandwidth is a much better match for $e_{33} \sim 1.1$ C/m² for the deposited AlN film.

Table I lists some critical parameters used in the simulations. As a first approximation, this work assumes frequency-independent loss parameters. The loss parameters, or the damping ratio in the material, are set to match the measured insertion loss and quality factor of several filters on the wafer. These parameters are kept constant throughout the analysis presented in this work.

A significant advantage of finite element simulations over existing analytical techniques is the ability to predict secondary and spurious resonance modes with reasonable accuracy. Figs. 7(a) and 7(b) illustrate the measured and simulated second- and third-order thickness-mode responses (as seen in the broadband response of the filter shown in Part I), showing a good agreement. To verify the general applicability of the model, the performance of a few devices on a particular die were also compared

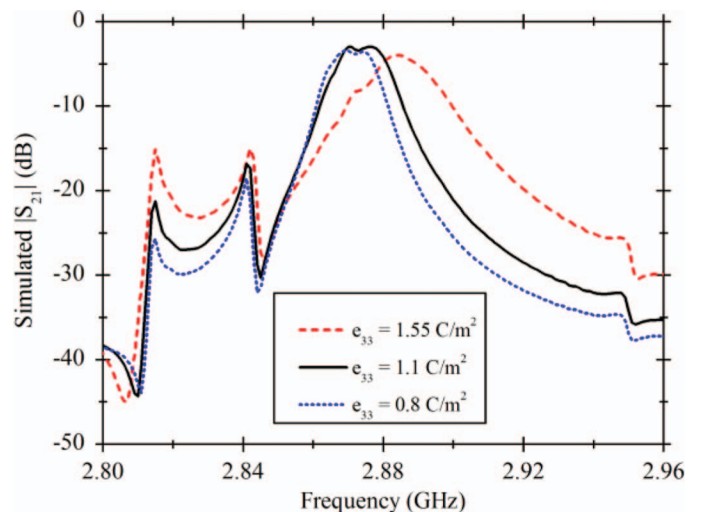


Fig. 6. Simulated $|S_{21}|$ of the filter under varying AlN piezoelectric stress coefficient e_{33} . A reduced e_{33} of 1.1 C/m² is seen to best match the measured bandwidth and roll-off. The frequency shift seen with the increase in e_{33} may be attributed to the piezoelectric stiffening effect.

TABLE I. PARAMETERS USED IN THE FINITE ELEMENT SIMULATIONS.

	Acoustic damping	Dielectric loss tangent	Effective ϵ_{33}
AlN	0.0015	0.001	1.1 C/m ²
Silicon	0.0005	—	—

against simulations. Fig. 8 presents the results, showing good agreement between the measured and simulated response of these devices.

III. DESIGN GUIDELINES

Fundamentally, the TPoS filter arrangement draws inspiration from the monolithic coupled resonator filter (MCF) configuration implemented with quartz crystals [17]. Similar filter structures replacing quartz with grown or deposited piezoelectric layers have also been investigated and simplified analytical expressions have been presented for them [8], [18]. Recently, a model was presented that analyzed acoustically coupled filters using superposition of eigenmodes [7], along the lines of earlier work on quartz-based filters [9]. Although this method is intuitive, it lacks sufficient detail needed to compute the accurate response of such coupled resonator filters.

In the previous section, we verified the accuracy and general applicability of our simulation model. Here, we use the same model to obtain the frequency response of TPoS filters under varying geometric parameters for the interdigitated electrodes. Based on the results obtained, we provide some design guidelines for achieving low-loss filters with different percentage bandwidths.

A. Center Frequency

The center frequency has a strong dependency on the film thickness, which is expected because the device operates in its thickness mode. For a given stack, the trapping

range is fixed by the cutoff frequencies of the electroded and the unelectroded regions (see Part I) and defines the frequency range in which a filter response may be designed. Therefore, varying lateral geometries can only marginally shift the center frequency of the filter.

B. Bandwidth and Insertion Loss

Fig. 9 shows the effect of varying interdigitated electrode spacing and number of electrode fingers on (a) the bandwidth and (b) the insertion loss of the filter. For this analysis, the electrode width is kept constant at 10 μm . The three curves represent three different electrode spacing values (3, 5, and 7 μm). The bandwidth (taken at half power, or 3 dB) is seen to increase as the electrode spacing is decreased. This is due to the stronger acoustic coupling between the electroded regions because the coupling is inversely proportional to the width of the coupling region (i.e., the region without electrodes on top). From Fig. 9, it can be seen that for a given electrode width and spacing, the bandwidth remains fairly constant with a large number of electrode fingers (number of electrode fingers >32). However, as the number of fingers is increased beyond a certain point (40 in this case), the size of the device becomes too large and additional resonance modes corresponding to longer lateral wavelengths can be excited, resulting in larger passband ripples and degrading the insertion loss [Fig. 10(a)]. Therefore, to obtain a low-loss and ripple-free passband, the electrode spacing must be reduced and the number of electrode fingers must be optimized.

A similar analysis is done to obtain the effect of variations in the electrode width. Fig. 11 presents the simulated bandwidth and insertion loss as a function of the number of electrode fingers, keeping the spacing constant at 5 μm for three different electrode widths (10, 12.5, and 15 μm). As seen from Fig. 11, a smaller electrode width provides a wider bandwidth. From the dispersion curves shown in Part I, we can expect that as the electrode width

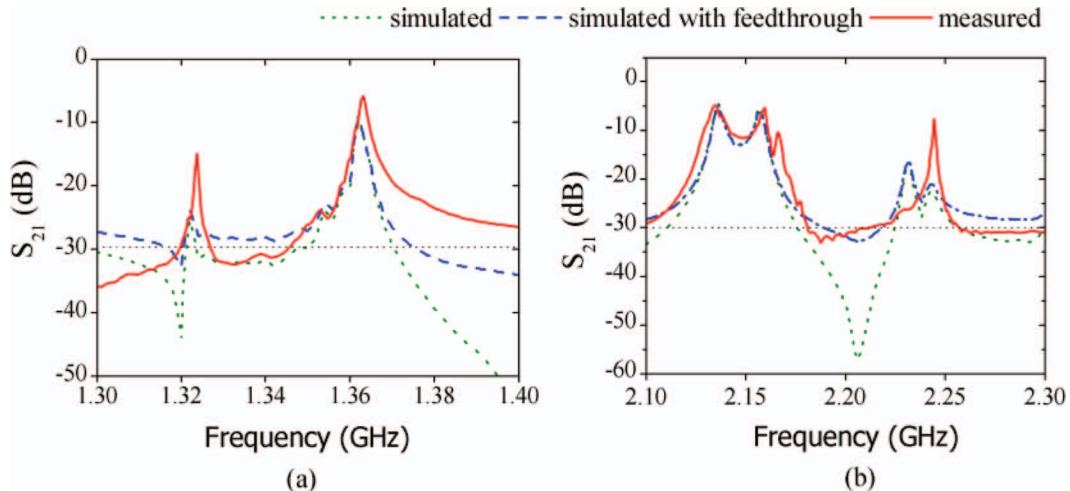


Fig. 7. Simulated and measured filter response for (a) second- and (b) third-order thickness mode of resonance. 

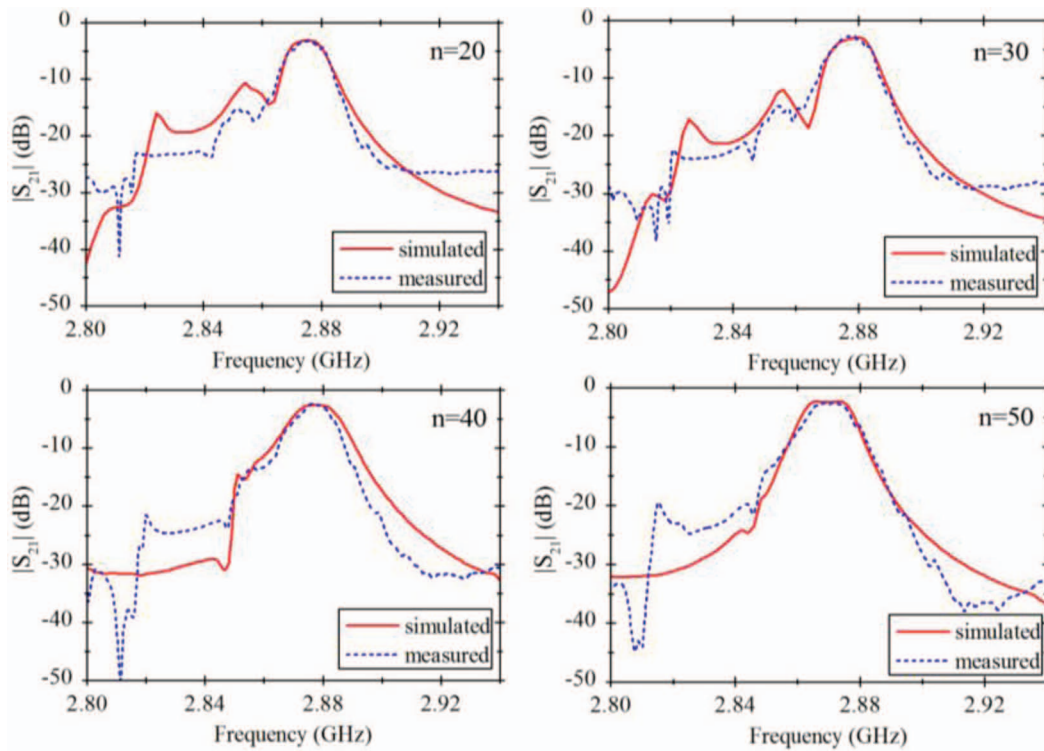


Fig. 8. Comparison between the measured and simulated filter responses. All filters are on the same die. n is the number of electrode fingers. All devices have an electrode width in the range of 9.8 to 10.2 μm and finger spacing in the range of 4.8 to 5.2 μm , with number of electrode fingers as shown in the plots. The actual thicknesses of the AlN and silicon layers, as well as electrode dimensions, were measured using scanning electron microscopy and used in these simulations. AlN e_{33} of 1.1 C/m² is used in these simulations.

decreases, frequencies of both the in-phase and the out-of-phase modes increase as a result of the shortened lateral wavelength. However, because the shift in the out-of-phase frequency is larger than the in-phase one, the resulting bandwidth is wider. More reduction of the electrode width causes the two resonance modes to move further away, and the passband ripple increases (beyond 3 dB; see Fig. 12). An electrode width of ~ 10 μm can provide a wide bandwidth without producing a large ripple in the passband. In general, smaller electrode spacing and narrower elec-

trode width with sufficient number of electrodes produce a wider bandwidth and a lower insertion loss. In addition to the top electrode geometries, the piezoelectric coupling coefficient e_{33} of AlN plays an important role on determining the passband ripple and the bandwidth [Fig. 10(b)].

Fig. 12 depicts the effect of top electrode geometry on the filter response, visualizing the results presented in Figs. 9 and 11. As shown, with the same stack thickness and material properties, the bandwidth of the filter can be designed to be anywhere between 0.2% and 1%, having

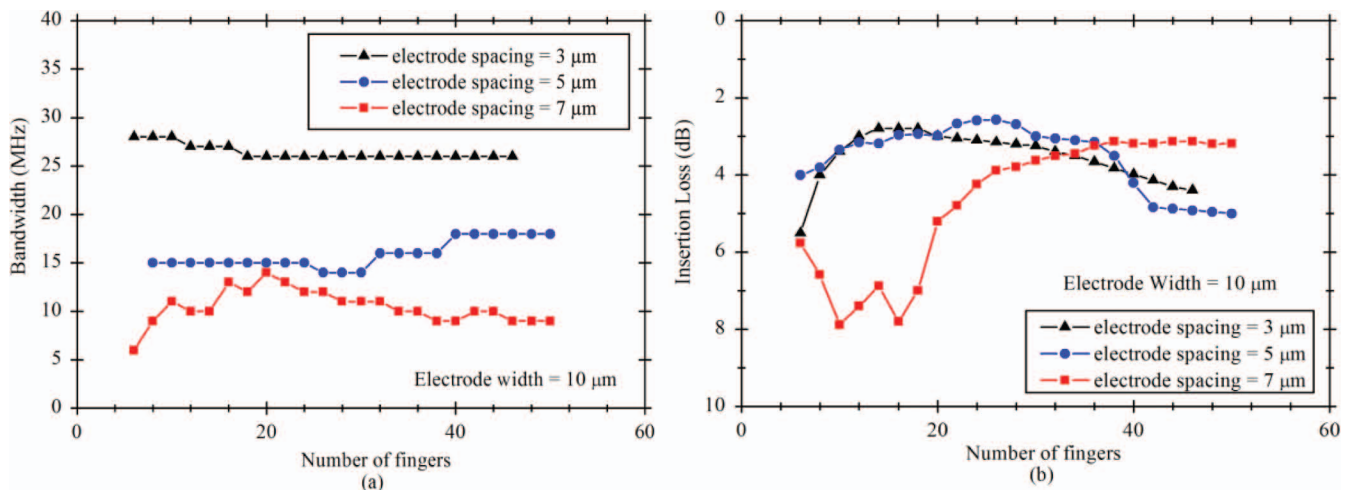


Fig. 9. Simulated filter (a) bandwidth and (b) insertion loss versus number of fingers for different spacing between electrode fingers. The electrode width is kept constant at 10 μm . All filters are centered at ~ 2.9 GHz.

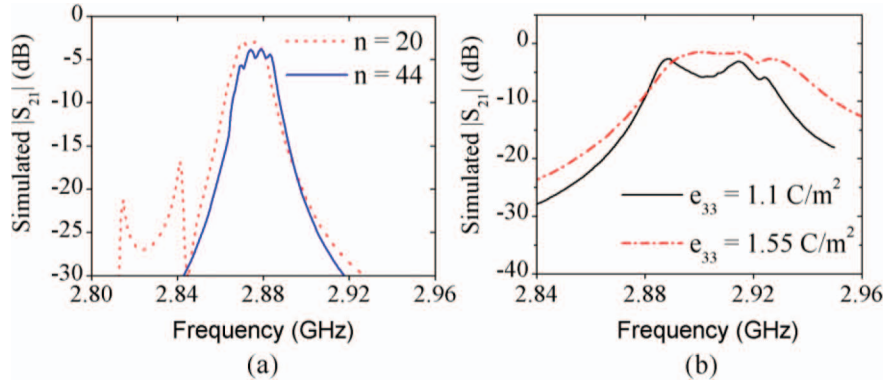


Fig. 10. (a) Simulated filter response for $n = 20$ and $n = 44$ showing the generation of additional unwanted resonances in the passband as the number of fingers is increased beyond 40. For both curves, the top electrode has a width of $10\ \mu\text{m}$ and spacing of $5\ \mu\text{m}$. (b) Simulated effect of reduced piezoelectric stress constant in AlN. For both curves, the top electrode consists of 20 electrodes, each $5\ \mu\text{m}$ wide and having a spacing of $5\ \mu\text{m}$.

an insertion loss of less than 5 dB and passband ripple of less than 1 dB. The ripple can be reduced by changing the thickness of the top electrode, as shown in Fig. 13. Increasing the electrode thickness results in a smaller bandwidth and a flatter passband, because of the higher energy trapping in the electroded regions and smaller coupling between them. Further increase in the electrode thickness (beyond an optimum value) results in increased insertion loss, as shown in Fig. 13 (inset).

In an earlier work on acoustically coupled ZnO-on-Si TPoS filters, it was shown that the bandwidth increased as the number of electrode fingers was increased [10]. In that work, the total device area and the electrode spacing were kept constant and the number of interdigitated electrode fingers was gradually increased. This implies that the electrode width decreases as the number of fingers increases. To verify this observation, simulations were setup for AlN filters and the results are plotted in Fig. 14. It can be seen that the bandwidth indeed increases as the number of fingers is increased from 26 to 44 but this trend does not hold for other regions of the plot. A similar simulation was performed with ZnO. Similar to AlN, the bandwidth of ZnO-on-Si filters is seen to be a function of

the number of fingers, having a positive slope only in a specific range. Depending on the stack material and geometric configuration, the range of fingers for which such a relation is seen varies. Thus, by adjusting the number of fingers, the bandwidth of the filter can be controlled to some extent.

To observe the effect of the thickness ratio of silicon to AlN on the filter bandwidth, simulations were performed with thickness ratio of 3:1 and results are compared with the presented work, i.e., thickness ratio of 5:1. For both cases, the AlN film thickness is taken to be $1\ \mu\text{m}$ and thus the Si layer thicknesses are 3 and $5\ \mu\text{m}$, respectively. The top electrode layout is kept the same in both cases and an exemplary result is plotted in Fig. 15. From the two curves, a larger frequency separation between the in-phase and out-of-phase modes and thus a wider bandwidth can be seen for a lower Si to AlN thickness ratio.

IV. CONCLUSION

We presented a simulation model using commercial FEA software applicable to the design and analysis of acoustically-coupled piezoelectric filters. The simulated

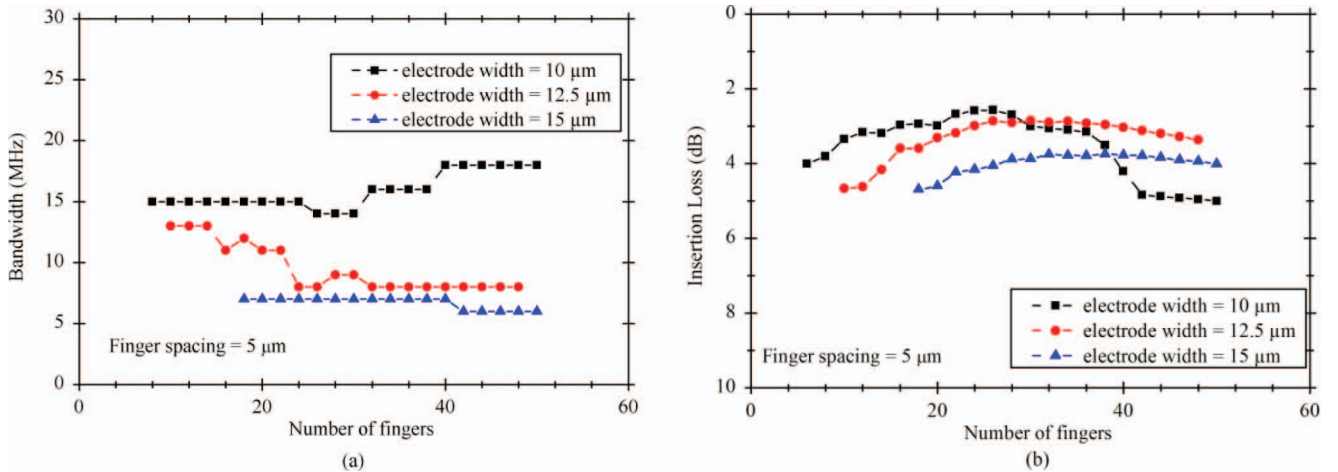


Fig. 11. Simulated filter (a) bandwidth and (b) insertion loss versus number of fingers for different electrode widths. The electrode spacing is kept constant at $5\ \mu\text{m}$. All filters are at $\sim 2.9\ \text{GHz}$.

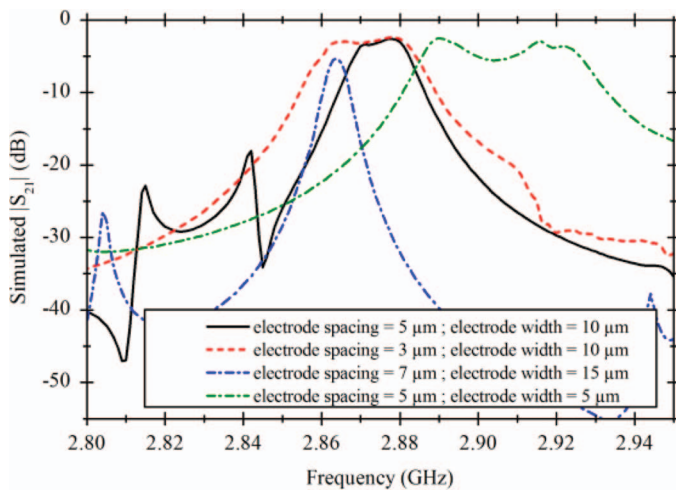


Fig. 12. Simulated filter response indicating the effect of electrode width and electrode spacing. The top electrode layout is as marked. The number of electrode fingers is 20 in all cases.

response of an interdigitated thickness-mode AlN-on-Si filter agrees well with the measured results presented in Part I using an effective e_{33} of 1.1 C/m^2 for AlN. Using the fitted parameters, plots presenting the effect of individual variables on the filter passband were presented and analyzed. It was shown, through simulations, that the inter-resonator coupling or the filter bandwidth can be varied by changing the top electrode geometry. This agrees well, in principle, with the theory presented in Part I. Therefore, tailoring the top electrode layout allows adjustment of the filter bandwidth, but it was shown to be eventually limited by the piezoelectric coupling of AlN. A maximum bandwidth of 1% is achievable with a piezoelectric coefficient, e_{33} , of only 1.1 C/m^2 and Si-to-AlN thickness ratio of 5:1. If required, wider bandwidths can be obtained if the quality of sputtered AlN is improved or

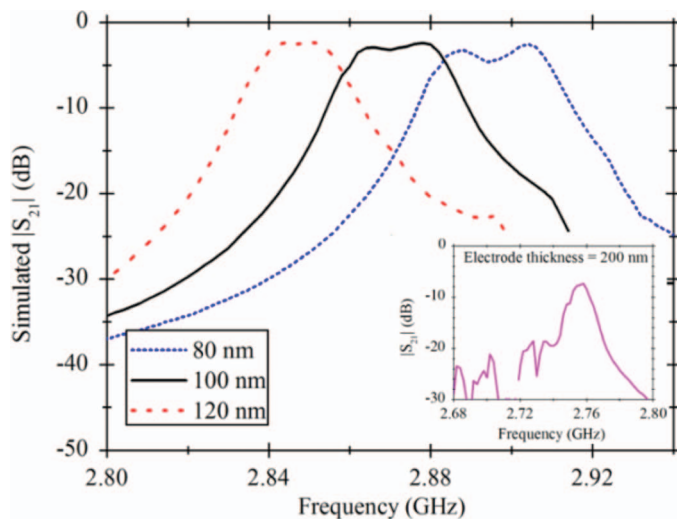


Fig. 13. Simulated response of a thickness-mode piezoelectric-on-substrate (TPoS) filter indicating the effect of the electrode thickness on the passband ripple. Increased electrode thickness improves the coupling and can reduce the ripple. Inset shows the filter response with electrode thickness of 200 nm.

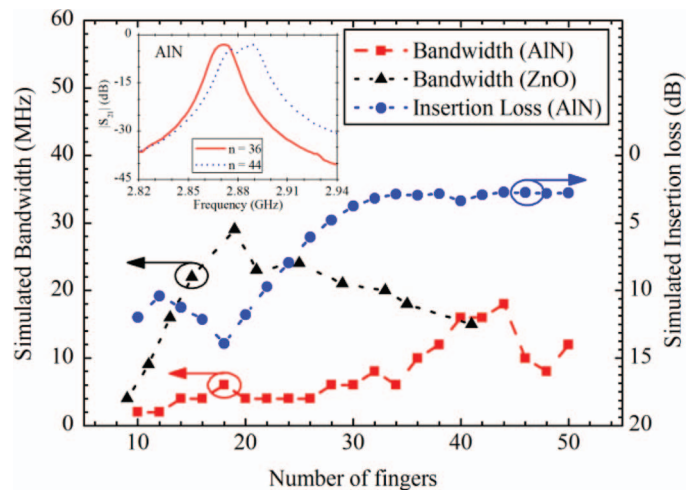


Fig. 14. Simulated filter bandwidth and insertion loss versus number of electrode fingers. For AlN-on-Si, the total device width is kept constant at $595 \mu\text{m}$ and interdigitated finger spacing is fixed at $5 \mu\text{m}$. For ZnO, the device width is $260 \mu\text{m}$ and finger spacing is $3 \mu\text{m}$. In both cases, as the number of fingers is increased, the electrode width is decreased. The results for AlN are at $\sim 2.9 \text{ GHz}$, whereas those for ZnO are at $\sim 1.8 \text{ GHz}$.

optimized Si-to-AlN thickness ratio is used. In general, it can be concluded that reducing interdigitated electrode width and finger spacing leads to a larger inter-resonator coupling, i.e., a wider bandwidth. Optimum designs based on these models can be expected to show a wide bandwidth with a low insertion loss.

Although earlier work on MCF topology provides some similar guidelines for the filter design, precise filter design without multiple fabrication trials has not been possible. Lack of analytical solutions in closed form for complex geometries led us to rely on finite element methods to determine the accurate frequency behavior of TPoS filters. With the development of the finite element analysis tool,

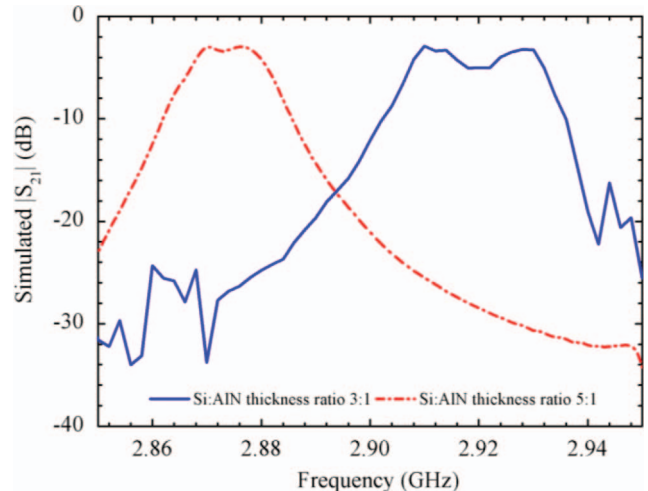


Fig. 15. Simulated effect of Si-to-AlN thickness ratio on the filter response. For both simulations, the top electrode geometry consists of 20 electrode fingers, each $10 \mu\text{m}$ wide with $5 \mu\text{m}$ spacing in between. The AlN film thickness is $1 \mu\text{m}$ in both cases. A wider bandwidth with a larger ripple can be clearly seen for the stack with reduced Si-to-AlN thickness ratio.

as shown in this paper, the time and cost of filter development are expected to be significantly reduced, making these filters viable for commercial applications.

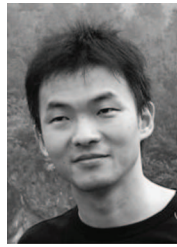
REFERENCES

- [1] W. P. Mason, *Electromechanical Transducers and Wave Filters*. New York, NY: Van Nostrand, 1942.
- [2] T. Makkonen, A. Holappa, J. Ellä, and M. M. Salomaa, "Finite element simulations of thin-film composite BAW resonators," *IEEE Trans. Ultrason. Ferroelectr. Freq. Control*, vol. 48, no. 5, pp. 1241–1258, 2001.
- [3] S. Morris and C. Hutchens, "Implementation of Mason's model on circuit analysis programs," *IEEE Trans. Ultrason. Ferroelectr. Freq. Control*, vol. 33, no. 3, pp. 295–298, 1986.
- [4] W. J. Spencer, "Monolithic crystal filters," in *Physical Acoustics*, 1974, vol. 9.
- [5] R. Abdolvand and F. Ayazi, "Monolithic thin-film piezoelectric-on-substrate filters," in *IEEE/MTT-S Int. Microwave Symp. Tech. Dig.*, 2007, pp. 509–512.
- [6] W. Pan, V. A. Thakar, M. Rais-Zadeh, and F. Ayazi, "Acoustically coupled thickness-mode AlN-on-Si band-pass filters—Part I: Principle and devices," vol. 59, no. 10, pp. 2262–2269, 2012.
- [7] T. Pensala, J. Meltaus, K. Kokkonen, and M. Yililammi, "2-D modeling of laterally acoustically coupled thin film bulk acoustic wave resonator filters," *IEEE Trans. Ultrason. Ferroelectr. Freq. Control*, vol. 57, no. 11, pp. 2537–2549, Nov. 2010.
- [8] H. F. Tiersten and D. S. Stevens, "An analysis of thickness-extensional trapped energy resonant device structures with rectangular electrodes in the piezoelectric thin film on silicon configuration," *J. Appl. Phys.*, vol. 54, no. 10, pp. 5893–5910, Oct. 1983.
- [9] R. Milsom, D. Elliot, S. Terry-Wood, and M. Redwood, "Analysis and design of coupled-mode miniature bar resonators and monolithic filters," *IEEE Trans. Sonics Ultrason.*, vol. 30, no. 3, pp. 140–155, 1983.
- [10] W. Pan, R. Abdolvand, and F. Ayazi, "A low-loss 1.8 GHz monolithic thin-film piezoelectric-on-substrate filter," in *Tech. Dig. IEEE MEMS Conf.*, 2008, pp. 176–179.
- [11] D. Bindel and S. Govindjee, "Elastic PMLs for resonator anchor loss simulation," *Int. J. Numer. Methods Eng.*, vol. 64, no. 6, pp. 789–818, Aug. 2005.
- [12] D. Pozar, *Microwave Engineering*. Reading, MA: Addison Wesley, 1990, pp. 217, 235.
- [13] Semiconductors on NSM. (2012, Jan.) [Online]. Available: <http://www.ioffe.ru/SVA/NSM/Semicond/index.html>
- [14] K. M. Lakin, "Coupled resonator filters," in *Proc. IEEE Ultrasonics Symp.*, 2002, pp. 901–908.
- [15] M. Dubois and P. Muralt, "Properties of AlN thin films for piezoelectric transducers and microwave filter applications," *Appl. Phys. Lett.*, vol. 74, no. 20, pp. 3032–3034, 1999.
- [16] M. Dubois and P. Muralt, "Stress and piezoelectric properties of aluminum nitride thin films deposited onto metal electrodes by pulsed direct current reactive sputtering," *J. Appl. Phys.*, vol. 89, no. 11, pp. 6389–6395, Jun. 2001.
- [17] J. F. Black, R. A. Courtney, T. W. Grudkowski, P. T. Norusis, and H. R. Wood, "Fundamental, longitudinal, thickness mode bulk wave resonators," U.S. Patent 4320365, Mar. 16, 1982.
- [18] D. V. Shick and H. F. Tiersten, "An analysis of thickness-extensional trapped energy mode transducers," *IEEE Ultrasonics Symp.*, 1982, pp. 509–514.



Vikram Thakar (S'12) is a doctoral candidate in the Department of Mechanical Engineering at the University of Michigan. He received his B.E. degree in mechanical engineering from the University of Pune, India, in 2006 and his M.E. degree in integrated microsystems from the University of Michigan, Ann Arbor, in 2011. His research interests are in the areas of resonant micromechanical devices, acoustically coupled micromechanical resonators, and piezoelectrically actuated resonators for oscillator applications. The main focus of

his research is on the relation between device modeling and fabrication as applied to the MEMS domain.



Wanling Pan (S'04–M'06) was born in 1980. He received his B.E. degree in electronic engineering from Tsinghua University, China, in 2000, and his Ph.D. degree in electrical engineering from the Katholieke Universiteit Leuven, Belgium, in 2006. From 2006 to 2009, he was a postdoctoral fellow in the School of Electrical and Computer Engineering, Georgia Institute of Technology, Atlanta, GA. He is currently with Integrated Device Technology Inc., San Jose, CA. His research interests include the design, fabrication, and characterization of MEMS devices, with a focus on micro-resonators and filters.



Farrokh Ayazi (S'96–M'00–SM'05) is a Professor in the School of Electrical and Computer Engineering at the Georgia Institute of Technology and a director of the Center for MEMS and Microsystems Technologies (CMMT) at Georgia Tech. He received the B.S. degree in electrical engineering from the University of Tehran, Iran, in 1994 and the M.S. and Ph.D. degrees in electrical engineering from the University of Michigan, Ann Arbor, in 1997 and 2000, respectively. His research interests are in the areas of integrated micro and

nano electromechanical resonators, inertial sensors, and interface IC design for MEMS and sensors. Dr. Ayazi is an editor for the *IEEE/ASME Journal of Microelectromechanical Systems*, and the *IEEE Transactions on Electron Devices*. He is a 2004 recipient of the NSF CAREER Award, the 2004 Richard M. Bass Outstanding Teacher Award (determined by the vote of the ECE senior class), and the Georgia Tech College of Engineering Cutting Edge Research Award for 2001–2002. He and his students won the best paper awards at Transducers 2011, the IEEE International Frequency Control Symposium in 2010, and IEEE Sensors conference in 2007.

Dr. Ayazi is the Co-Founder and Chief Technology Officer of Qualtré Inc., a spin-out from his research laboratory that commercializes multi-axis bulk acoustic wave silicon gyroscopes and six-degrees-of-freedom inertial sensors for consumer electronics and personal navigation systems.



Mina Rais-Zadeh (S'03–M'08) received the B.S. degree in electrical engineering from the Sharif University of Technology, Tehran, Iran, and the M.S. and Ph.D. degrees in electrical and computer engineering from the Georgia Institute of Technology, Atlanta, GA, in 2005 and 2008, respectively. From August 2008 to 2009, she was a Postdoctoral Research Fellow with the Integrated MEMS Group, Georgia Institute of Technology. Since January 2009, she has been with the University of Michigan, Ann Arbor, where she is currently an

Assistant Professor in the Department of Electrical Engineering and Computer Science. Her research interests include passive micromachined devices for communication applications, resonant micromechanical devices, gallium nitride MEMS, and micro/nano fabrication process development. Prof. Rais-Zadeh is the recipient of the NSF CAREER Award in 2011, the IEEE Electron Device Society Early Career Award in 2011, and finalist in the student paper competitions at the SIRF (2007) and IMS (2011) conferences. She serves as a member of the technical program committees of IEEE IEDM, IEEE Sensors, and the Hilton Head workshop.